Predictive deconvolution of multiple free surface in marine seismic data

Raimundo N. C. Carneiro, Lourenildo W. B. Leite*, Wildney. W. S. Vieira* and Cleudilene S. Rufino, UFOPA, UFPA*, Brazil

Abstract

The present research aimed to the analysis and mitigation of multiple free surface from to the systematic study of multiple unobstructed view of the prediction filter based on the theory of communication in order to better apply the filter deconvolution WH predictive. Migrated sections were obtained in time and depth where it allows the interpretation.

Introduction

The predictive deconvolution is normally used in seismic procesing data with the objective to comprime the seismic pulse or predict the multiple reflections.

The main objective here is to couple a prediction-attenuation model based process, with the result analyzed by comparison between the input and the output. The data is described as a random process, and the Wiener-Hopf operator is designed by taking into account a probabilistic distribution for the error difference between the desired and real output (Peacook and Treitel, 1969; Robinson and Treitel, 1969; Robinson, 1984; Makhoul, 1978; Berkhout and Zaanen, 1979; Mesko, 1984). The efforts were not only around the filter theory, but first in the prediction strategy. The infinite possibilities to describe multiple paths are constrained to the amplitude variation due to the reflection and transmission coefficients; that is, these internal coefficients are rather small, as a result the multiple paths have amplitudes small enough to be under the local noise amplitudes. Even thou, the multiple as a noise component can still have a correlation pattern.

A strategy was followed in this work, and resumed as:

1. Spheric divergence correction;

2. Organization of CMP families;

3. Velocity analysis;

4. Normal-moveout correction

5. Predicitive deconvolution

6. Stack

7. Kirchhoff migration

Predictive Filter

The filter coefficients are obtained from the solution to an optimization problem in the least-square sense, where the object function is given by the expectation of the distribution of errors, $e(h_j)$, between desired, z_k, and real, y_k, outputs:

$$e(h_j) = E\{(z_k - y_k)^2\}, \tag{1}$$

to be minimized as function of the h_j coefficients. This means to search for the minimum variance, as $E\{(z_k - y_k)\} = 0$. The filter output, y_k, is given by the convolution between h_k and the observed input g_k as:

$$y_k = \sum_{i=0}^{P-1} h_i g_{k-i}, \qquad (k = 0,1,2,...,N-1, \Delta t = 1). \tag{2}$$

For the minimization, the criteria is that the partial derivatives with respect to the h_j coefficients be null, what means that the the searched point in parameter space is close to the solution,

$$\frac{\partial e(h_j)}{\partial h_j} = 0. \tag{3}$$

The partial derivative operation results in the normal linear WH equation:

$$\sum_{i=0}^{P-1} h_i \phi_{gg}(j-i) = \phi_{zg}(j), \qquad (j = 0,1,2,...,P-1). \tag{4}$$

The quantity $\phi_{gg}(j-i)$ is the autocorrelation of the input g_k. The $\phi_{zg}(j)$ is the unilateral positive part of the theorectical crosscorrelation between the desired output, z_k, and the real output, z_k. The principle applied to construct the WH equation allows for several practical operations, but we restrict to the so called Predictive Operator. The matrix structure corresponding to equations (4) has the form:

$$
\begin{pmatrix}
A_{00} & A_{01} & \cdots & A_{0,P-1} \\
A_{10} & A_{11} & \cdots & A_{1,P-1} \\
\vdots & \vdots & \vdots & \vdots \\
A_{P-1,0} & A_{P-1,1} & \cdots & A_{P-1,P-1}
\end{pmatrix}
\begin{pmatrix}
h_0 \\ h_1 \\ \vdots \\ h_{P-1}
\end{pmatrix}
=
\begin{pmatrix}
c_0 \\ c_1 \\ \vdots \\ c_{P-1}
\end{pmatrix}
\tag{5}
$$

WH Prediction Filter

In the present model the desired output is $z_k = g_{k+T}$. Therefore, z_k is a prediction of g_k at a time distance T, in this way we have:

$$
\begin{pmatrix}
A_{00} & A_{01} & \cdots & A_{0,P-1} \\
A_{10} & A_{11} & \cdots & A_{1,P-1} \\
\vdots & \vdots & \vdots & \vdots \\
A_{P-1,0} & A_{P-1,1} & \cdots & A_{P-1,P-1}
\end{pmatrix}
\begin{pmatrix}
h_0 \\ h_1 \\ \vdots \\ h_{P-1}
\end{pmatrix}
=
\begin{pmatrix}
A_T \\ A_{T+1} \\ \vdots \\ A_{T+P-1}
\end{pmatrix}
\tag{6}
$$

where h_k is called prediction error operator, and h_k^* is the prediction operator defined by:

$$h^* = [1,\overbrace{0,0,...,0,0}^{(T-1)zeros},-h_0,-h_1,-h_2,...,-h_{N-1}]. \quad (7)$$

NMO method

The methodology consisted of specific steps and organized with titles of NMO method. A commom property to these two methods is the use commom-mid-point (CMP) families, that are caracterized by the reciprocity principle source-sensor, and consequently not solving for dips. Another commom property is the semblance measure of coherence along the trajectories, $t(h)$ and $t(x_m,h)$, of the sum of traces to produce the stack CMP sections.

The beginning of this work was with the normal-moveout (NMO) correction and stack that is based on the model formed by flat, homogeneous and isotropic layers, where the transit time for the primary reflections is given by the hyperbolic approximation (8) (Hubral and Krey, 1980):

$$t(h) = \sqrt{t^2(0) + \frac{(2h)^2}{v^2}}; \quad (8)$$

where the independent variable h is the half-offset source-receiver; $t(0)$ is the double-time relative to the normal incidence in zero offset; v is the search paramenter, where $v = v_{NMO}$ defines a velocity for the normal-moveout time correction, stack and to estimate the v_{RMS} velocity (root mean square). Therefore, this model is to be considered as initial, since it only considers vertical variation of velocity within the aperture established for the calculation. A next more complex model considers layers with dipping interfaces, but still admitting CMP families and the semblance measure.

In the NMO case, the analysis of the v parameter is performed based on the CMP family, by picking pairs of (v_{NMO},t_0) in the semblance coherence section calculated with equation (9), where the values of $S(t_0,\mathbf{m})$ vary in the range $(0,1)$ (Sguazzero and Vesnaver, 1987):

$$S(t_0,\mathbf{m}) = \frac{1}{N} \frac{\sum_{t=t_0-\delta t/2}^{t_0+\delta t/2}\left[\sum_{h=h_1}^{h_2}\bar{u}(h,t;t_0,\mathbf{m})\right]^2}{\sum_{t=t_0-\delta t/2}^{t_0+\delta t/2}\sum_{h=h_1}^{h_2}[\bar{u}(h,t;t_0,\mathbf{m})]^2}, \quad (9)$$

where $\bar{u}(h,t;t_0,\mathbf{m})$ represents the processed trace amplitude positioned along the path of the subtended sum of equation (8); N is the number of involved traces; $\mathbf{m}$ are the trajectory function parameters, $t(h;t_0,\mathbf{m})$. The sum along $t(h)$ and is defined within a spatial-temporal window where is selected a curve that best represents the reflection event. In the NMO case, the search parameter is only the velocity named $v = \mathbf{m} = v_{NMO}$ that, depending on the application, can be expressed mathematically by the v_{RMS} velocity.

Results

For this case the water layer velocity (v_0) and geometry (angle α and segment position) is previously known, and the configuration for the modeling is as shown in Figure 1,

that shows the sea floor approximated by linear segments. For this dipping topographical model, the multiples can be Normal or Oblique (Olhovich, 1964).
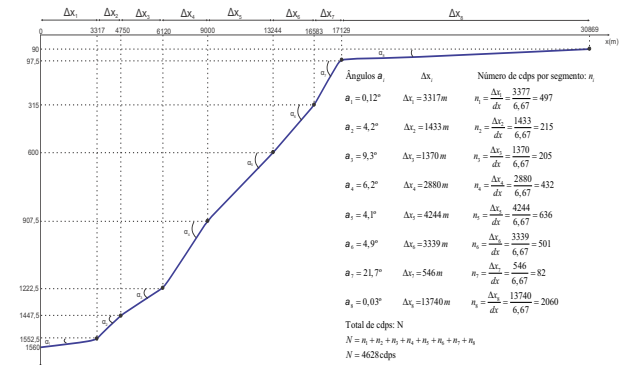

Figure 1: Division of the continental platform in segments for the line Camamu 5519.

This strategy was implemented by Carneiro (2013), where the normal trajectory between sensor (at the marine free surface normal multiples) and the vertical to the sea floor (approximated by the minimum offset information) is given by equation (10):

$$t_n(x=0;k,\alpha) = 2k\frac{h}{v_0 \text{sen}\alpha}\text{sen}(n+1)\alpha \quad (10)$$

where n is the number of reverberations, k is the multiple order, α is the reflector topographical dip, and h the vertical thickness. The Normal multiples repeat themselves in a reverberation process (between source and receptor points), but the oblique do not repeat and propagate toward the deeper ocean.

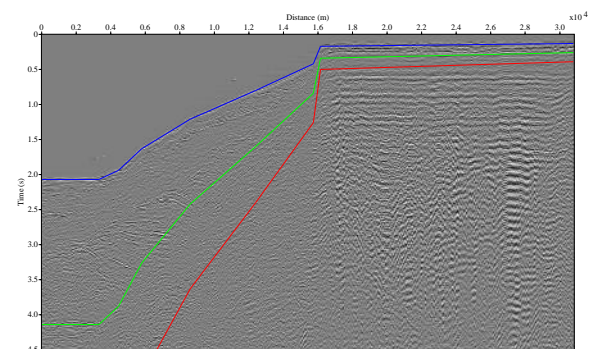The reflections time of the normal multiples are shown in the Figure 2.

Figure 2: Minimum offset section from line Camamu 5519. The blue line corresponds to the tracing of the primary reflection, the green line to the first free surface multiple, the red line to the second and starts around 6.3s.

NMO corrected sections

A Figura 4 mostra o mapa semblance onde os pares (v_{NMO},t_0) devem ser marcados em conjunto com a análise dos eventos de reflexāo, e cada evento é relacionado a um par que melhor o horizontaliza.
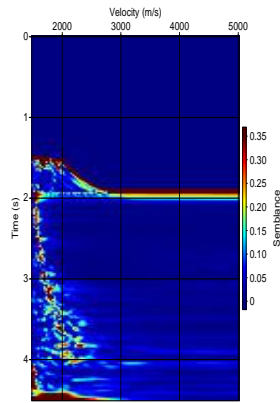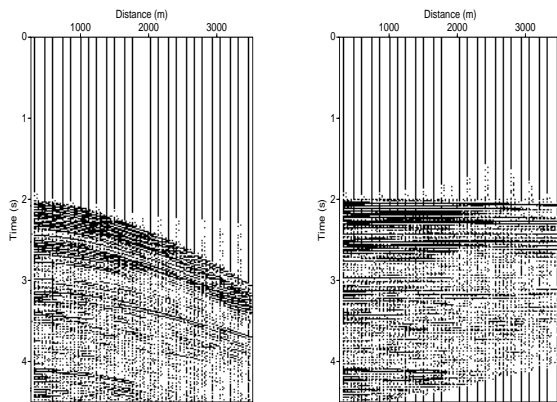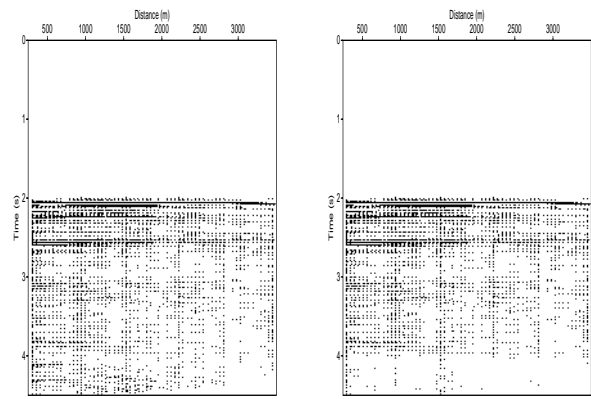
Figure 3: Semblance map for CMP 450.

Figure 4: CMP 450 before (left), and after the NMO correction (right).

Adopted coefficients of the WH filter

Table 1 shows a selected sample of the primary tracing, and the correspondent multiple for all CMPs, as a result of applying the method based on equation (10). These observed traveltimes are the ones necessary to obtain the WH filter coefficients for the predictive deconvolution.

Table 1: Data for the multiple trace.

CDP's	Segment (m)		Primary (s)	Multiple (s)
1-497	1°	0-3317	2.07	4.14
498-713	2°	3317-4750	1.93	3.86
714-919	3°	4750-6120	1.63	3.26
920-1352	4°	6120-9000	1.21	2.42
1353-1989	5°	9000-13244	0.80	1.60
1990-2491	6°	13244-16583	0.42	0.84
2492-2575	7°	16583-17129	0.13	0.34
2576-4628	8°	17129-30800	0.12	0.26

Practical application of the WH filter in the NMO sections.

Figure 5 shows CMPs 400 (above) and 450 (below), before (left) and after (right) the predictive multiple deconvolution, respectively.

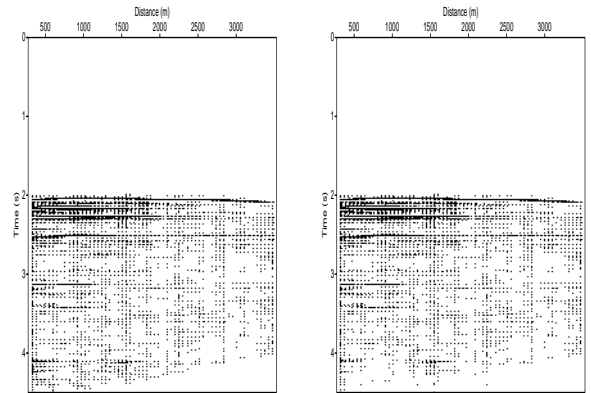Figure 6 shows the velocity model NMO in time used im the NMO stack.

Figure 5: NMO section, CMPs 400 and 450 before and after the application of the multiple predictive deconvolution. We observe the constant periodicity of the multiple reflection, and its attenuation around 4.14s, showing the good result obtained from the deconvolution process.
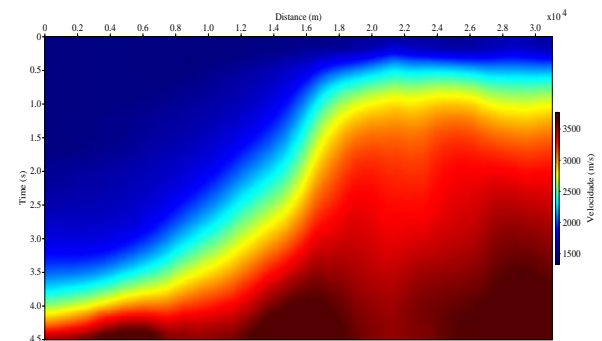

Figure 6: The dark blue color is related to the low and the red to the higher velocities.

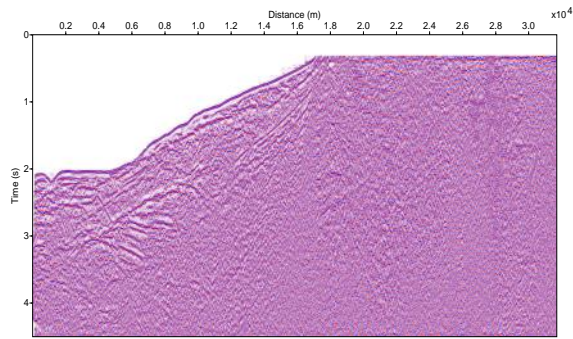Figure (7) shows the stack section after the application of the WH deconvolution.

Figure 7: NMO stack section of Camamu line L5519 using manual picking in the semblance map, where we can see that the major part of the registered information corresponds to shallow events, and the reflections have good trace-to-trace correlation giving good continuity.We also observe the multiple attenuation in the inferior left part of the section around 4.14s, and showing that the deconvolution experiment gave satisfactory results.

In this work we performed a post-stack time Kirchhoff migration (Schneider (1978)) using vRMS(t) a velocity model shown in Figure 6 obtained from the semblance velocity analysis, where the major coherence reflection events were picked. Analyzing this section (see Figure 8) we can see that the structures of the subsurface shift a little with respect to stack section of Figure 7.

The time migration section obtained in this work is shown also in Figure 8.
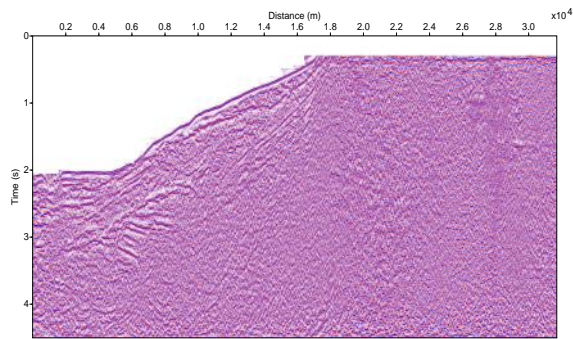

Figure 8: Post stack time Kirchhoff migration of Camamu line L5519, form NMO stack section of Figure 7, and using the RMS velocity model of Figure 6. We can observe the partial diffraction collapse, and the recover of reflection events in the deeper time part of the section. But, we observe arc structures over the diffraction points in the deeper time parts of the section

The RMS time velocity model was converted to depth using Dix-Durbaum transform to interval velocity, and the result is shown in Figure 9.

We have also converted the time stack section to depth by a change of scale of the time axis, where the the stack velocity has been previously resampled form time to depth, as shown in Figure 9. The time stack to depth stack is shown in Figure 10.

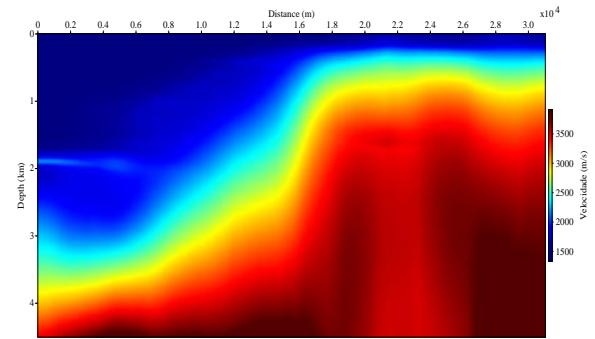Figure 11 shows the depth migration section, where we

Figure 9: Depth velocity distribution map of Camamu line L5519 obtained from Figure 6 by conversion of $vrms(t)$ to $vint(z)$ velocity.
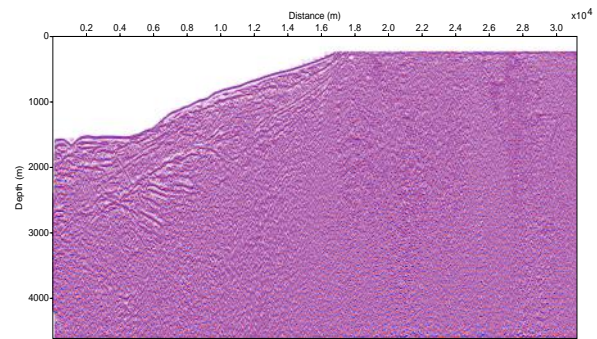

Figure 10: NMO stack (see Figure 7) of Camamu line L5519 rescaled to depth using the velocity model of Figure 9,using a linear interpolation and a constant extrapolation on the semblance map to determine the $vint(z)$ velocities for non specified intervals. Observe that the section was rescaled only to the depth of 4612m.

observe the diffraction collapse, as well as the recovering of several reflection events showing a better result than the time migration.
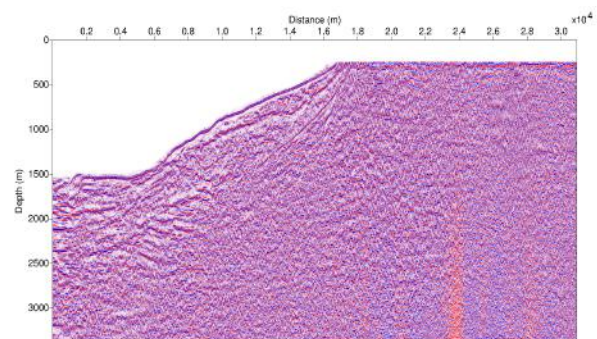

Figure 11: Kirchhoff depth migration of Camamu line L5519 from the NMO stack section (see Figure 11) using the velocity model of Figure 9. We see the recovering of subhorizontal structures traced by the better continuity of reflection events, the diffraction collapse, lineament as geological faulting, the recovering of several reflectors at deeper time part of the section, and the absence of arcs over the diffraction points ("smile types"), existent in the migration of Figure 8. Due to further geological information, the considered depth was 3.380m. The migration aperture parameter was taken as 300m.

Conclusions

The WH operator for the case of predictive multiple deconvolution in time domain was designed for marine seismic sections, where the periodicity parameter needs strong a priori information about the topography of the sea continental platform, from where we trace the primary and the multiple, according to the Normal or Oblique case. The operator was designed to predict the multiple, and the result showns in Figure 6. The velocity analysis was performed in the semblance map for reflection events on 92 CDPs, from a total of 4628 CDPs. The obtained velocity model is presented in Figure 6, where we observe the structure of the continental slope.

The multiple attenuation was performed on the data after the NMO correction, once the events were flattened, and the result can be seen in Figure 5, where we can see the multiple attenuation in sections of CMP 400 and 450. We observe that the filter has a good performance for small offsets, mas less resolution as the offset increases. As a conclusion, we need to review this work looking for an operator that changes the performance wit offset distance, in order to take care of the pulse stretching. A natural procedure is to perform time stack after deconvolution, and the result is present in Figure 7. We observe a meaningful increase in the S/N ratio, where the shallow events are highlighted, and the free surface multiple attenuation acts in the 4s window. A post-stack time Kirchhoff migration shown in Figure 8, that was obtained from the stack section of Figure 7, using the velocity model of Figure 6. The conclusion was for the partial collapse of some diffraction events, and the recovering of depth reflection events. But, still undesirable arc shape events are present in the deeper parts of the section. Also, a scale change of time-to-depth for the NMO stack of Figure 10. For this, it was used the interval velocity model of Figure 9 from a linear interpolation, and a constant extrapolation for points picked in the semblance map to determine the $vint(z)$ velocities for non specified time intervals. In this case the section was rescaled to 4612m depth.

Acknowledgements

References

Berkhout, A. J., and Zaanen, P. R., 1979, A comparison between wiener filtering, kalman filtering and deterministic least squares estimation: Geophysical Prospecting, **24**, no. 3, 141–197.

Carneiro, R. N. C., 2013, Marcação e atenuação de múltiplas de superfície livre, processamento e imageamento de dados sísmicos marinos: Master's thesis, Universidade Federal do Pará.

Hubral, P., and Krey, T., 1980, Interval velocities from seismic reflection time measurements: Society of Exploration Geophysicists, Tulsa, OK.

Makhoul, J., 1978, Linear prediction: a tutorial review:, pages 99–118.

Mesko, A., 1984, Digital filtering: Application in geophysical exploration for oil: Pittman Advanced Publishing Program.

Olhovich, V., 1964, The causes of noise in seismic reflection and refraction work.:, **29**, no. 06, 1015–1030.

Peacook, K., and Treitel, L., 1969, Predictive deconvolution: Theory and practice: Geophysics, , no. 34, 155–169.

Robinson, E. A., and Treitel, S., 1969, Predictive deconvolution: Theory and practice: Geophysics, **34**, no. 2, 155–169.

Robinson, E., 1984, Seismic inversion and deconvolution: Geophysical Press. London.

Schneider, W. A., 1978, Integral formulation for migration in two-dimensions and three-dimensions:, **43**, no. 01, 49–76.

Sguazzero, P., and Vesnaver, A., 1987, A comparative analysis of algorithms for stackincg velocity estimation: deconvolution and inversion: Oxford: Blackwell Scientific Publications,.